CrystEngComm

ROYAL SOCIETY OF CHEMISTRY

PAPER

View Article Online
View Journal | View Issue

Cite this: *CrystEngComm*, 2024, **26**, 3844

A lanthanide metal–organic framework containing a hydrazine group for highly sensitive luminescent sensing of formaldehyde gas†

Wenqian Cao,‡ Fangying Teng,‡ Yuanjing Cui * and Guodong Qian *

Received 24th April 2024,
Accepted 7th June 2024

DOI: 10.1039/d4ce00406j

rsc.li/crystengcomm

The determination of formaldehyde (HCHO) concentration in human exhaled breath can be used as an effective means for the early diagnosis of lung cancer. Lanthanide metal–organic frameworks (LnMOFs) have shown great potential in formaldehyde fluorescence sensing, yet challenges persist in achieving high sensitivity and selectivity. In this work, we report new hydrazine-functionalized LnMOFs (Ln = Eu^{3+}, Gd^{3+}, Tb^{3+}, $H_2BDC–NH–NH_2$ = 2-hydrazine-terephthalic acid), having an *fcu* topology for the sensitive and selective detection of formaldehyde gas. The ligands with hydrazine groups not only act as an "antenna effect" between the ligands and Eu^{3+} ions, but also act as formaldehyde recognition sites, enabling Eu-$BDC–NH–NH_2$ to be used for fluorescence enhanced sensing of formaldehyde gas in gaseous environments. Eu-$BDC–NH–NH_2$ thus exhibits low detection limit (41.7 ppb), high selectivity, and fast (3 minutes) formaldehyde gas response, showing great potential to be practically applied in the field of early diagnosis of lung cancer.

1. Introduction

Given the high incidence and mortality rates of lung cancer, there is an urgent need for a rapid, non-invasive diagnostic method for early detection of lung cancer.[1,2] Exhaled breath analysis is closely linked to diverse metabolic activities in the human body and plays a crucial role in the development of lung cancer.[3,4] In particular, the concentration of formaldehyde in the exhaled breath of lung cancer patients is approximately 83 parts per billion (ppb), significantly surpassing that of healthy individuals (48 ppb).[5] The development of a straightforward and highly sensitive quantitative detection method for formaldehyde gas in exhaled breath is crucial for enabling early diagnosis of lung cancer. Conventional analytical methodologies, including mass spectrometry, high-performance liquid chromatography, and gas chromatography, can provide reliable results but usually require expensive instruments and the usage of large amounts of solvents.[6,7] Fluorescence sensing technology has attracted much attention for its advantages such as simple operation, high sensitivity, fast response speed and strong anti-interference ability.[8] However, the reported formaldehyde fluorescence probe materials primarily including small organic molecules, quantum dots, and carbon dots commonly face challenges related to poor stability, high detection limits, and complex synthesis processes.[9,10] Therefore, designing a fluorescent probe with a low detection limit, high selectivity, and specificity for formaldehyde gas in gaseous environments remains a significant challenge.

Lanthanide metal–organic frameworks (LnMOFs)[11–15] are crystalline porous materials assembled from lanthanide-containing nodes or clusters and organic ligands, combining not only the luminescence properties of lanthanide (*e.g.*, long fluorescence lifetime, large Stokes shift and characteristically sharp line emissions) but the unique advantages of MOFs (*e.g.*, high porosity, high specific surface area and functional tunability). Owing to these excellent characteristics, LnMOFs have garnered significant attention and research in the fields of temperature,[16–18] ions,[19–22] organic molecules[23,24] and pH sensing.[25,26] The porous structure and multifunctionality of MOFs provide an ideal platform for the enrichment and selective recognition of analytes. Nevertheless, due to the limited interaction between formaldehyde gas and MOFs in gaseous environments, numerous chemical reactions that typically occur in solution are impeded, thereby resulting in the current Ln-MOFs lacking effective strategic guidance for achieving high selectivity in the detection of formaldehyde gas.[27–31] Introducing specific functional sites and designing reactive fluorescent probes can improve the selectivity and

State Key Laboratory of Silicon and Advanced Semiconductor Materials, ZJU-Hangzhou Global Scientific and Technological Innovation Center, School of Materials Science & Engineering, Zhejiang University, Hangzhou 310027, China. E-mail: cuiyj@zju.edu.cn, gdqian@zju.edu.cn

† Electronic supplementary information (ESI) available: Supplementary figures and table of the characterization of the as-prepared nanoparticles. CCDC 2348622. For ESI and crystallographic data in CIF or other electronic format see DOI: https://doi.org/10.1039/d4ce00406j

‡ These authors contributed equally to this paper.

recognition ability of specific analytes. By virtue of the high reactivity of the hydrazine group towards formaldehyde gas, it can be utilized as a functional site to enrich formaldehyde gas based on the aldehyde–amine condensation reaction.[32–34] We thus present that the condensation reaction between hydrazine groups and formaldehyde gas, along with the exceptional luminescence performance of LnMOFs, can be harnessed to develop a reactive fluorescence probe for formaldehyde gas. This innovative approach aims to overcome the challenges of low sensitivity and specificity encountered with traditional fluorescence probes used in gas sensing.

To verify this hypothesis, we herein utilize 2-hydrazine-terephthalic acid (H_2BDC–NH–NH_2) containing hydrazine groups as organic ligands and Ln^{3+} (Ln = Eu^{3+}, Gd^{3+}, Tb^{3+}) ions to construct new lanthanide metal–organic frameworks Ln-BDC–NH–NH_2 (Scheme 1). The efficient energy transfer from H_2BDC–NH–NH_2 to Eu^{3+} ions results in the sharp characteristic emissions of Eu^{3+} ions in Eu-BDC–NH–NH_2. When Eu-BDC–NH–NH_2 is exposed to formaldehyde gas, the characteristic emissions of Eu^{3+} ions are significantly enhanced. As expected, the hydrazine groups within Eu-BDC–NH–NH_2 can undergo condensation reactions with formaldehyde gas. The generation of hydrazone compounds further enhances the energy transfer from the ligands to Eu^{3+} ions, thereby enabling Eu-BDC–NH–NH_2 to exhibit high sensitivity and specific turn-on fluorescence sensing of formaldehyde gas in a gaseous environment. Importantly, the detection limit is as low as 41.7 ppb, which is significantly lower than the formaldehyde level in the exhaled breath of lung cancer patients (83 ppb), showing great potential to be practically applied in the field of early diagnosis of lung cancer.

2. Experimental methods

2.1 Synthesis of Ln-BDC–NH–NH_2 (Ln = Eu^{3+}, Gd^{3+}, Tb^{3+})

0.073 mmol of $Eu(NO_3)_3{\cdot}6H_2O$, 0.073 mmol of 2-hydrazine-terephthalic acid (H_2BDC–NH–NH_2) and 0.586 mmol of 2-fluorobenzoic acid (2-FBA) were ultrasonically dissolved in a 20 ml screw glass bottle containing 3.65 ml DMF and 0.6 ml deionized water. After the addition of 0.05 ml nitric acid (3.5 M in DMF), the glass bottle was placed in a constant temperature oven at 105 °C for 3 days. After the reaction, it was slowly cooled to room temperature, filtered, and washed with DMF and anhydrous ethanol several times. The synthesis process of Gd-BDC–NH–NH_2 or Tb-BDC–NH–NH_2 was similar to Eu-BDC–NH–NH_2 except that the metal salt $Eu(NO_3)_3{\cdot}6H_2O$ was replaced with $Gd(NO_3)_3{\cdot}6H_2O$ or $Tb(NO_3)_3{\cdot}6H_2O$.

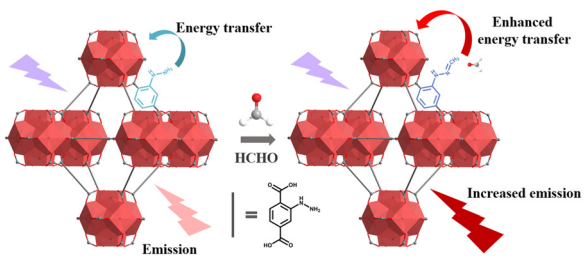

Scheme 1 Schematic diagram of Eu-BDC–NH–NH_2 fluorescence enhanced sensing of formaldehyde gas.

2.2 Activation of Eu-BDC–NH–NH_2

The synthesized Eu-BDC–NH–NH_2 (50 mg) was immersed in anhydrous methanol (20 ml) for 3 days, and the solvent was exchanged every 12 hours. Then after being filtered and activated at 80 °C under vacuum for 1 day, the activated Eu-BDC–NH–NH_2 was obtained.

2.3 Detection of formaldehyde gas by Eu-BDC–NH–NH_2

Different volumes of 37% formaldehyde solution were dropped into different bottles. After a long time of sufficient free volatilization, the concentration of formaldehyde gas in the bottle reached equilibrium, so as to set a series of formaldehyde gas of different concentrations (0–1000 ppb). The concentration of formaldehyde gas was calculated using eqn (1)

$$C_{ppm} = \frac{V_l \times V_m \times D}{4 \times V_c \times MW} \quad (1)$$

where C_{ppm} = concentration of formaldehyde gas in the bottle, V_l = volume of 37% formaldehyde solution dropped into the bottle, V_m = molar volume of formaldehyde (1 atm, 25 °C), D = gas density of formaldehyde, V_c = volume of the bottle, and MW = molecular weight of formaldehyde.

The prepared Eu-BDC–NH–NH_2 powder was affixed to the glass sheet and then the glass sheet was placed vertically in the fluorescence spectrometer to test the initial fluorescence spectra. The bottles containing formaldehyde gas of different concentrations were quickly turned upside down on the glass sheet. After waiting for a period of time to ensure that Eu-BDC–NH–NH_2 powder fully reacted with formaldehyde gas *in situ*, the bottles were removed and the *in situ* fluorescence spectra were quickly tested and recorded.

3. Results and discussion

3.1 Design and characterization of Ln-BDC–NH–NH_2

Based on the hydrothermal method, a series of isostructural Ln-BDC–NH–NH_2 (Ln = Eu^{3+}, Gd^{3+}, Tb^{3+}) were synthesized. The phase purity of the bulk sample is confirmed by powder X-ray diffraction (PXRD) between the simulated patterns and those of as-synthesized (Fig. 1a). The PXRD pattern is highly consistent with the simulated diffraction pattern obtained from the analysis of single crystal structure, which proves the successful synthesis of Ln-BDC–NH–NH_2 (Ln = Eu^{3+}, Gd^{3+}, Tb^{3+}) with good crystallinity and phase purity. Since these crystals are isostructural, herein we only depict the Tb-BDC–NH–NH_2 structure elaborately. Single-crystal XRD analysis reveals that Tb-BDC–NH–NH_2 crystallizes in the cubic system with the $Fm\bar{3}m$ space group (CCDC number: 2348622). Each Tb^{3+} ion is nine-coordinated, engaging four μ_3-OH and four O atoms derived from four distinct ligands, while the ninth

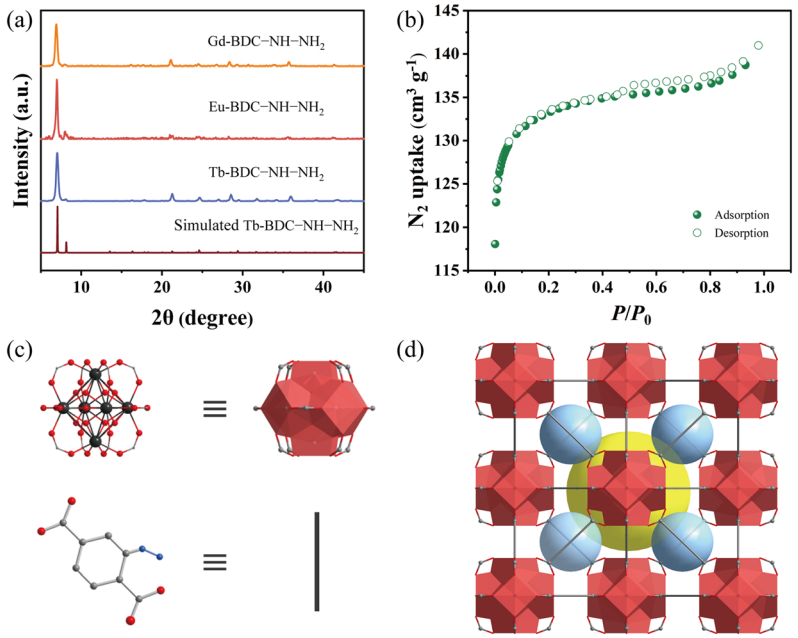

Fig. 1 (a) The PXRD of simulated Tb-BDC–NH–NH_2 and the as-synthesized Tb-BDC–NH–NH_2, Eu-BDC–NH–NH_2 and Gd-BDC–NH–NH_2. (b) The 77 K nitrogen adsorption and desorption curves of Eu-BDC–NH–NH_2. Schematic diagram of the crystal structure of Tb-BDC–NH–NH_2: (c) Tb_6 molecular building block [$Tb_6(\mu_3\text{-}OH)_8(COO^-)_{12}$] and 2-hydrazine-terephthalic acid (H_2BDC–NH–NH_2); (d) Tb-BDC–NH–NH_2 crystal structure along the *a*-axis.

coordination site is occupied by a water molecule. Adjacent Tb^{3+} ions are interconnected *via* μ_3-OH and fully deprotonated carboxyl groups to construct 12-connected secondary building units (SBUs), designated as [$Tb_6(\mu_3\text{-}OH)_8(COO^-)_{12}$] (Fig. 1c). These SBUs further assemble into a three-dimensional (3D) framework through the bridging of carboxyl groups within the organic ligands (Fig. 1d), thereby generating tetrahedral and octahedral cages. The metal cluster nodes are bridged with the carboxyl groups of the organic linkers, which upon periodic expansion and arrangement ultimately form a 3D face-centered cubic (*fcu*) topology. Table S1† lists the related crystallographic data and refinement parameters of Tb-BDC–NH–NH_2.

Bright and dark field micrographs of Eu-BDC–NH–NH_2 were taken using an inverted microscope (Fig. S1†). Eu-BDC–NH–NH_2 presented regular octahedra with clear edges, smooth surfaces and uniform and bright red light, and the crystal diameter is about 150 μm. The as-prepared Eu-BDC–NH–NH_2 was structurally examined based on single-crystal and powder XRD, elemental analyses, FTIR, TGA and BET studies. The FTIR spectra of organic ligands H_2BDC–NH–NH_2 and Eu-BDC–NH–NH_2 were measured. As shown in Fig. S2,† the ligand shows a vibration absorption peak belonging to the carbonyl groups at 1690 cm^{-1}, while after the formation of Eu-BDC–NH–NH_2, two new absorption peaks appeared at 1600 cm^{-1} and 1395 cm^{-1} from the antisymmetric and symmetric stretching vibrations of deprotonated $–COO^-$, indicating the coordination of –COOH and Eu^{3+} ions. The thermal stability of Eu-BDC–NH–NH_2 was assessed by TGA. As shown in Fig. S3,† the thermal decomposition process of Eu-BDC–NH–NH_2 can be divided into two stages: the first weight loss in the 30–490 °C range is 27.76%, which can be mainly attributed to the removal of residual water and DMF molecules from the surface and pores of the crystal. A rapid decrease in the weight occurs in the second stage when the temperature rises to 500 °C, which corresponds to the decomposition of ligands in Eu-BDC–NH–NH_2. The TGA curve showed that Eu-BDC–NH–NH_2 can maintain structural stability up to 500 °C. For the requirement of formaldehyde gas sensing in a gaseous environment, Brunauer–Emmett–Teller (BET) gas absorptiometry measurements were conducted to examine the porous nature of Eu-BDC–NH–NH_2. The N_2 adsorption/desorption isotherm of Eu-BDC–NH–NH_2 shown in Fig. 1b are identified as type I, which is characteristic of microporous materials. The BET specific surface area of Eu-BDC–NH–NH_2 is calculated to be about 543.5 m^2 g^{-1}, which can provide enough space for formaldehyde molecules to enter and fully interact with the hydrazine groups in Eu-BDC–NH–NH_2.

3.2 Luminescence properties

Solid-state excitation and emission spectra of ligand H_2BDC–NH–NH_2 and Eu-BDC–NH–NH_2 are shown in Fig. S6† and 2a. When excited at 320 nm, H_2BDC–NH–NH_2 exhibits a broad emission at 381 nm, which is attributed to the π–π* electron transition of the ligands. Under the excitation at 326 nm, Eu-BDC–NH–NH_2 exhibits a very weak ligand emission centered at 429 nm and strong and sharp characteristic emissions at 578, 591, 615, 652 and 698 nm, which correspond to the

electron transition of Eu^{3+} ions at $^5D_0 \rightarrow {}^7F_J$ (J = 0–4), respectively. The single emission characteristic of Eu-BDC–NH–NH_2 is due to the efficient "antenna effect" of the ligands to Eu^{3+} ions.

The low-temperature (77 K) time-resolved phosphorescence (TRPL) spectra of isomorphic Gd-BDC–NH–NH_2 were measured in order to further interpret the energy transfer process in Eu-BDC–NH–NH_2. As shown in Fig. S5a,† Gd-BDC–NH–NH_2 exhibited a wide emission centered at 438 nm, and the red shift of the ligand emission can be attributed to the coordination between the ligands and Gd^{3+} ions. The lowest excited state $^6P_{7/2}$ of Gd^{3+} (32 000 cm^{-1}) is too high to accept energy from the triplet excited energy level (T_1) of H_2BDC–NH–NH_2, the phosphorescence of Gd-BDC–NH–NH_2 results from the ligands, thus T_1 of H_2BDC–NH–NH_2 is calculated to be about 22 173 cm^{-1} shown in Fig. S5b.† The energy transfer process between the ligands and Eu^{3+} ions is shown in Fig. 2b, and the energy gap between T_1 and Eu^{3+} excited state ($^5D_1$ = 19 030 cm^{-1}) is 3143 cm^{-1}, lying within 2500–3500 cm^{-1} and satisfying the optimal energy transfer based on Latva's empirical rule, which showed the high energy transfer efficiency of the ligands to Eu^{3+} ions. The ligands efficiently sensitize Eu^{3+} ions through the energy transfer process, leading to the predominant characteristic emission of Eu^{3+} ions in Eu-BDC–NH–NH_2.

3.3 Fluorescence sensing of formaldehyde gas

To evaluate the application potential of Eu-BDC–NH–NH_2 as a formaldehyde fluorescence sensor in a gaseous environment, the fluorescence responses of Eu-BDC–NH–NH_2 to formaldehyde gas were investigated. With the exposure to increasing concentrations of formaldehyde gas, the fluorescence of Eu^{3+} ions in Eu-BDC–NH–NH_2 was enhanced (Fig. 3a). The fluorescence intensity changes of Eu-BDC–NH–NH_2, defined as $I/I_0 - 1$ (I and I_0 are the fluorescence intensity ($^5D_0 \rightarrow {}^7F_2$) of Eu^{3+} ions before and after exposure to formaldehyde gas), and the concentrations of formaldehyde gas (0–1000 ppb) can be well fitted to a function of $I/I_0 - 1 = -0.477 \times \exp(-C_{HCHO}/307.271) - 0.476 \times \exp(-C_{HCHO}/307.300) + 0.957$ (R^2 = 0.998) (Fig. 3b). When the concentration range of formaldehyde gas is 0–80 ppb, the fluorescence intensity changes of Eu-BDC–NH–NH_2 can be linearly fitted with the concentrations of formaldehyde gas (R^2 = 0.981) (Fig. 3c). The limit of detection (LOD) can be calculated from the formula LOD = $3\delta/K_{SV}$, where δ is the standard deviation of 20 times blank experiments (Fig. S6†) and K_{SV} is the slope of the linear fitting equation. The LOD was 41.7 ppb, which was significantly lower than the concentration of formaldehyde in the exhaled breath of lung cancer patients (83 ppb), indicating Eu-BDC–NH–NH_2 to be a potential fluorescence sensor for quantitative detection of low concentration formaldehyde gas in human exhaled breath. The sensitivity of Eu-BDC–NH–NH_2 outperforms that of several other MOF-based formaldehyde fluorescence sensors reported to date (Table S2†).

Human exhaled breath is a complex gas environment containing hundreds of volatile organic/inorganic compounds, which requires high selectivity of formaldehyde fluorescence sensors. Therefore, we investigated the fluorescence response of Eu-BDC–NH–NH_2 to various common species in human exhaled breath, including water, *n*-hexane, acetone, ammonia, formaldehyde, alcohols and monoaromatic hydrocarbons (MACHs). The fluorescence spectra of Eu-BDC–NH–NH_2 were recorded after being exposed to a series of different gas environments *in situ* for 1 minute. As shown in Fig. S7, S8† and 3d, other gases have little influence on the fluorescence intensity of Eu-BDC–NH–NH_2 except for formaldehyde gas. When exposed to formaldehyde gas, the fluorescence intensity of Eu-BDC–NH–NH_2 at 615 nm exhibited a significant enhancement (Fig. 3d), unequivocally indicating the high selectivity and specificity of Eu-BDC–NH–NH_2 for formaldehyde gas.

To realize real-time disease monitoring, the fluorescence sensors necessitate rapid response speed. Therefore, the time response characteristics of Eu-BDC–NH–NH_2 to formaldehyde gas sensing were explored. We recorded the time-dependent emission spectra of Eu-BDC–NH–NH_2 when exposed *in situ* to

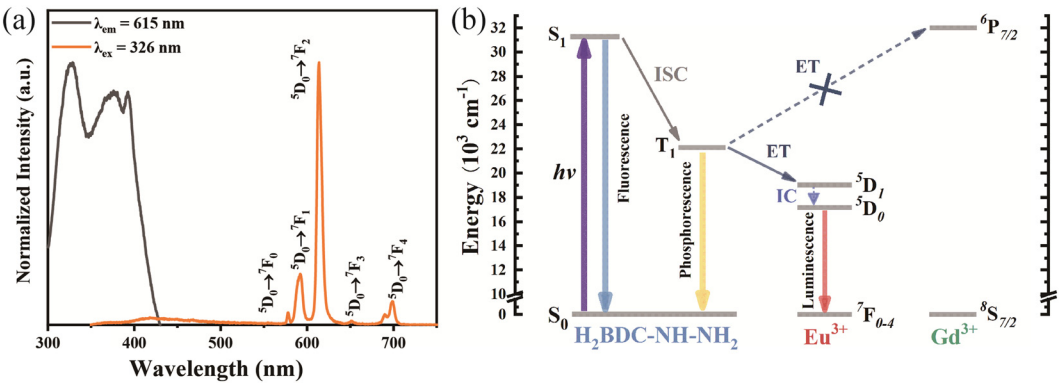

Fig. 2 (a) Solid-state excitation and emission spectra of Eu-BDC–NH–NH_2. (b) Diagram of the energy transfer process between ligands and Ln^{3+} (Eu^{3+} and Gd^{3+}).

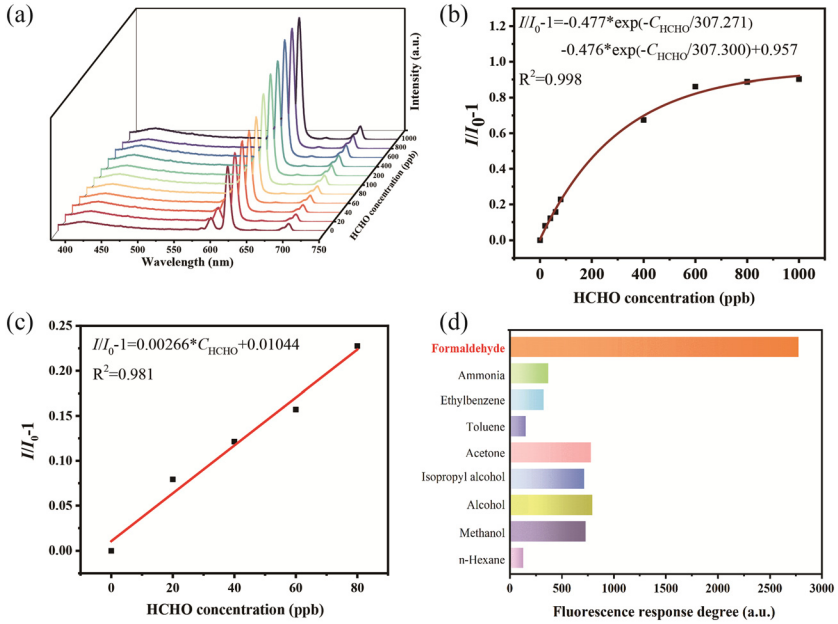

Fig. 3 (a) Emission spectra of Eu-BDC–NH–NH_2 exposed to increasing concentrations of HCHO gas (0–1000 ppb). (b) Fitted curve and (c) linear relationship of the fluorescence intensity of Eu-BDC–NH–NH_2 enhanced by HCHO gas. (d) The fluorescence response degree (I – I_0) of Eu-BDC–NH–NH_2 at 615 nm after being exposed to different gases (λ_{ex} = 326 nm).

200 ppb formaldehyde gas. As shown in Fig. S9,† the fluorescence intensity of Eu-BDC–NH–NH_2 at 615 nm showed a fast and obvious trend of enhancement over time. The fluorescence enhancement effect surpassed 90% after 2 minutes and remained nearly constant after 3 minutes, demonstrating that Eu-BDC–NH–NH_2 exhibits a rapid response to formaldehyde gas through the aldehyde–amine condensation reaction.

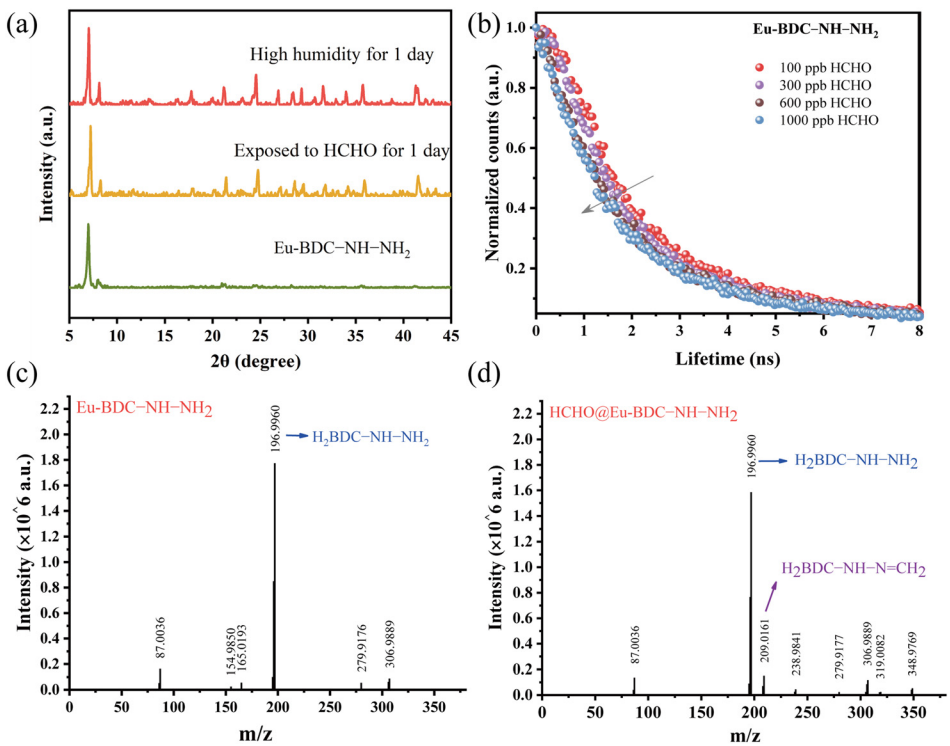

Fig. 4 (a) PXRD patterns of Eu-BDC–NH–NH_2 in a high humidity environment and formaldehyde gas environment for 1 day. (b) Time-resolved radioluminescence decay curves at 440 nm emission of Eu-BDC–NH–NH_2 reacting with different concentrations of formaldehyde gas. Mass spectrum of Eu-BDC–NH–NH_2 (c) before and (d) after being exposed to HCHO gas.

3.4 Sensing mechanism of Eu-BDC–NH–NH_2

The excellent fluorescence sensing of Eu-BDC–NH–NH_2 to formaldehyde gas is due to the high reactivity of free hydrazine groups to formaldehyde. The hydrazone compounds formed during the aldehyde–amine condensation reaction affect the luminescence of Eu-BDC–NH–NH_2. We first investigated the structural stability of Eu-BDC–NH–NH_2 during the detection process. As shown in Fig. 4a the PXRD pattern of Eu-BDC–NH–NH_2 after being exposed to high concentration of formaldehyde gas for 24 hours corresponded well with the simulated Eu-BDC–NH–NH_2, which proved that the structure of Eu-BDC–NH–NH_2 remained well in the process of detecting formaldehyde gas.

To explore the aldehyde–amine condensation reaction mechanism in detail, FTIR and UV-vis were used to measure Eu-BDC–NH–NH_2 before and after exposure to formaldehyde. As shown in Fig. S2,† after being exposed to formaldehyde gas, the characteristic absorption peak at 665 cm^{-1} from primary amines disappeared, indicating that the formaldehyde gas was bound to the free hydrazine groups. The UV-vis spectra of the Eu-BDC–NH–NH_2 suspension in anhydrous methanol in the presence of formaldehyde solution were recorded (Fig. S10†). With the gradual increase of formaldehyde concentration, two new absorption peaks appeared in the range of 220–245 nm and 265–290 nm, indicating the interaction between formaldehyde and hydrazine groups. In order to further prove the formation of hydrazone compounds, the mass spectrometry of Eu-BDC–NH–NH_2 before and after the detection of formaldehyde gas was recorded. As shown in Fig. 4c and d, the peak observed at m/z = 196.9960 corresponds to the organic ligand H_2BDC–NH–NH_2. After the exposure to formaldehyde gas, a new peak appeared at m/z = 209.0161 in the mass spectrometry of HCHO@Eu-BDC–NH–NH_2, which belongs to the hydrazone compounds formed during the aldehyde–amine condensation reaction of the free hydrazine groups with formaldehyde (H_2BDC–NH–N═CH_2). Combining the above results, it can be concluded that the free hydrazine groups in Eu-BDC–NH–NH_2 react with formaldehyde gas during the detection process, and the formed hydrazone compounds can promote the energy transfer process between the ligands and Eu^{3+} ions, resulting in enhanced fluorescence of Eu-BDC–NH–NH_2. After reacting with formaldehyde gas, the fluorescence lifetime of the ligands in Eu-BDC-NH-NH_2 decreases. With an increase in formaldehyde gas concentration, a noticeable decrease in fluorescence lifetime is observed (Fig. 4b). As shown in Fig. S11,† the initial lifetime of 5.04 ns decreased to 3.0 ns after reacting with formaldehyde gas, a change of nearly 40%, proving the enhancement of the energy transfer process. This result further demonstrates the enhanced energy transfer process from the ligands to Eu^{3+} ions, resulting in intensified emission intensity of Eu^{3+} ions.

4. Conclusion

In conclusion, new lanthanide metal–organic frameworks Ln-BDC–NH–NH_2 were synthesized by using hydrazine-modified ligand 2-hydrazine-terephthalic acid and Ln^{3+} (Ln = Eu^{3+}, Gd^{3+}, Tb^{3+}) ions. The hydrazine-functionalized Eu-BDC–NH–NH_2 exhibited the characteristic emission of Eu^{3+} ions owing to the "antenna effect" process. The hydrazine groups of Eu-BDC–NH–NH_2, serving as specific recognition sites for formaldehyde gas, undergo condensation reactions, enhancing the energy transfer process from the ligands to Eu^{3+} ions, thereby achieving fluorescence enhancement sensing of gaseous formaldehyde. Such a mechanism of the fluorescence response was confirmed by FTIR, mass spectra and fluorescence lifetime analysis. Furthermore, Eu-BDC–NH–NH_2 showed high selectivity for formaldehyde gas, and could respond quickly within 3 minutes, with a detection limit as low as 41.7 ppb. This work therefore may provide a strategy to design and functionalize LnMOFs for highly sensitive detection of formaldehyde gas, offering new opportunities for early diagnosis of lung cancer.

Author contributions

Wenqian Cao: conceptualization, methodology, and writing – review & editing. Fangying Teng: conceptualization, methodology, data curation, and writing. Yuanjing Cui and Guodong Qian: supervision, funding acquisition, project administration, and writing – review & editing.

Conflicts of interest

There are no conflicts to declare.

Acknowledgements

This work was supported by the National Natural Science Foundation of China (52025131) and the Science Technology Department of Zhejiang Province (2023C01098 and 2024C01191).

Notes and references

1 R. Nooreldeen and H. Bach, *Int. J. Mol. Sci.*, 2021, **22**, 8661.
2 G. Yang, Z. Xiao, C. Tang, Y. Deng, H. Huang and Z. He, *Biosens. Bioelectron.*, 2019, **141**, 111416.
3 P. C. Moura, M. Raposo and V. Vassilenko, *Clin. Chim. Acta*, 2024, **552**, 117692.
4 T. Chen, T. Liu, T. Li, H. Zhao and Q. Chen, *Clin. Chim. Acta*, 2021, **515**, 61–72.
5 A. T. Güntner, V. Koren, K. Chikkadi, M. Righettoni and S. E. Pratsinis, *ACS Sens.*, 2016, **1**, 528–535.
6 P. Shende, J. Vaidya, Y. A. Kulkarni and R. S. Gaud, *J. Controlled Release*, 2017, **268**, 282–295.
7 D. Marzorati, L. Mainardi, G. Sedda, R. Gasparri, L. Spaggiari and P. Cerveri, *J. Breath Res.*, 2019, **13**, 34001.
8 W. Dou, H. Han, A. C. Sedgwick, G. Zhu, Y. Zang, X. Yang, J. Yoon, T. D. James, J. Li and X. He, *Sci. Bull.*, 2022, **67**, 853–878.
9 R. Mohammadi, H. Naderi-Manesh, L. Farzin, Z. Vaezi, N. Ayarri, L. Samandari and M. Shamsipur, *J. Pharm. Biomed. Anal.*, 2022, **212**, 114628.

10 S. Sargazi, I. Fatima, M. Hassan Kiani, V. Mohammadzadeh, R. Arshad, M. Bilal, A. Rahdar, A. M. Díez-Pascual and R. Behzadmehr, *Int. J. Biol. Macromol.*, 2022, **206**, 115–147.
11 X. Wang, Y. Jiang, A. Tissot and C. Serre, *Coord. Chem. Rev.*, 2023, **497**, 215454.
12 Y. Zhao and D. Li, *J. Mater. Chem. C*, 2020, **8**, 12739–12754.
13 X. Li, S. Lu, D. Tu, W. Zheng and X. Chen, *Nanoscale*, 2020, **12**, 1521–1535.
14 S. Sun, Y. Zhao, J. Wang and R. Pei, *J. Mater. Chem. B*, 2022, **1**, 9535–9564.
15 J. Chen, M. Li, R. Sun, Y. Xie, J. R. Reimers and L. Sun, *Adv. Funct. Mater.*, 2024, 2315276.
16 D. Chen, N. Vankova, G. Jha, X. Yu, Y. Wang, L. Lin, F. Kirschhöfer, R. Greifenstein, E. Redel, T. Heine and C. Wöll, *Angew. Chem., Int. Ed.*, 2024, **63**, e202318559.
17 S. Wang, J. Jiang, Y. Lu, J. Liu, X. Han, D. Zhao and C. Li, *J. Lumin.*, 2020, **226**, 117418.
18 D. Andriotou, S. A. Diamantis, A. Zacharia, G. Itskos, N. Panagiotou, A. J. Tasiopoulos and T. Lazarides, *Molecules*, 2020, **25**, 523.
19 J. Li, Y. Zhu, H. Xu, T. Zheng, S. Liu, Y. Wu, J. Chen, Y. Chen and H. Wen, *Inorg. Chem.*, 2022, **61**, 3607–3615.
20 Q. Zhang, J. Wang, A. M. Kirillov, W. Dou, C. Xu, C. Xu, L. Yang, R. Fang and W. Liu, *ACS Appl. Mater. Interfaces*, 2018, **10**, 23976–23986.
21 H. Guo, N. Wu, R. Xue, H. Liu, L. Li, M. Wang, W. Yao, Q. Li and W. Yang, *Colloids Surf., A*, 2020, **585**, 124094.
22 C. A. Nagasaka, N. Ogiwara, S. Kobayashi and S. Uchida, *Small*, 2024, **20**, 2307004.
23 S. Sahoo, S. Mondal and D. Sarma, *Coord. Chem. Rev.*, 2022, **470**, 214707.
24 R. Yuan and H. He, *Inorg. Chem. Front.*, 2020, **7**, 4293–4319.
25 T. Feng, Y. Ye, X. Liu, H. Cui, Z. Li, Y. Zhang, B. Liang, H. Li and B. Chen, *Angew. Chem., Int. Ed.*, 2020, **59**, 21752–21757.
26 T. Xia, Y. Cui, Y. Yang and G. Qian, *ChemNanoMat*, 2017, **3**, 51–57.
27 J. Li, S. L. Yao, S. J. Liu and Y. Q. Chen, *Dalton Trans.*, 2021, **50**, 7166–7175.
28 Y. Zhang and B. Yan, *J. Mater. Chem. C*, 2019, **7**, 5652–5657.
29 W.-Q. Zhang, B. Zhang, T. Wang, J. Chen, Z.-Y. Li, R.-H. Wang, S. Liu and J.-J. Zhang, *J. Mater. Chem. A*, 2024, **12**, 7732–7741.
30 J. Li, X. Xiong, D. Luo, Y. Wei, W. Lu and D. Li, *Chem. Commun.*, 2022, **58**, 649–6493.
31 Y. Wei, M. Wang, D. Luo, Y. Huang, M. Xie, W. Lu, X. Shu and D. Li, *Mater. Chem. Front.*, 2021, **5**, 2416–2424.
32 J. Zheng, W. Liu, F. Lu, Y. Tang and Z. Yuan, *J. Anal. Test.*, 2022, **6**, 204–215.
33 S. Chen, X. Duan, C. Liu, S. Liu, P. Li, D. Su, X. Sun, Y. Guo, W. Chen and Z. Wang, *J. Hazard. Mater.*, 2024, **467**, 133672.
34 S. Nandi, E. Sharma, V. Trivedi and S. Biswas, *Inorg. Chem.*, 2018, **57**, 15149–15157.

